Supporting Information for "Seasonal discharge response to temperature-driven changes in evaporation and snow processes"

Joost Buitink[1], Lieke A. Melsen[1], and Adriaan J. Teuling[1]

[1]Hydrology and Quantitative Water Management Group, Wageningen University, Wageningen, Netherlands

Introduction

This supplement contains additional information to support the descriptions and explanations in the main manuscript. We include a brief description of the models, and their calibration procedure. We show metrics for both the calibration and validation period in all subbasins used in this study. Additionally, we explain how evaporation and snow variables responded to each incremental temperature increase, as we focus only on the most extreme case in the main manuscript.

Text S1, Model descriptions

Text S1.1, BETA

A simple soil moisture model (BETA, Beta EvapoTranspiration Adjustment) is used to preprocess the evaporation input, since dS2 requires actual evaporation input. This model simulates the rootzone, and determines evaporation reduction based on the amount of water stored in the rootzone. Actual evaporation is assumed to be a function of the available soil moisture such that:

$$ET_{\text{actual}} = ET_{\text{potential}} \cdot \beta(\theta), \tag{1}$$

where β represents the evaporation reduction parameter as a function of soil moisture θ. β is defined using three linear relations with θ, based on Laio et al. (2001):

$$\beta(\theta) = \begin{cases} \beta_{\text{w}} \frac{\theta - \theta_{\text{h}}}{\theta_{\text{w}} - \theta_{\text{h}}} & \text{if } \theta \leq \theta_{\text{w}} \\ \beta_{\text{w}} + (1 - \beta_{\text{w}}) \frac{\theta - \theta_{\text{w}}}{\theta_{\text{c}} - \theta_{\text{w}}} & \text{if } \theta_{\text{w}} \leq \theta \leq \theta_{\text{c}} \\ 1 & \text{if } \theta_{\text{c}} \leq \theta \leq \theta_{\text{s}} \end{cases} \tag{2}$$

where θ_{h} represents the hydroscopic point, θ_{w} the wilting point, θ_{c} the critical soil moisture content, θ_{s} the saturated soil moisture content, and β_{w} the fraction of reduced evaporation at wilting point.

Leakage from the rootzone is calculated to simulate the vertical movement of water. This water is assumed to be gone from the rootzone, as we do not simulate a layer below the rootzone. The leakage is simulated according to Clapp and Hornberger

(1978), integrated over time:

$$Q_{\text{leakage}} = L\theta_{\text{t}} - L\theta_{\text{s}} \left[\left(\frac{\theta_{\text{t}}}{\theta_{\text{s}}} \right)^{-2b-2} + \frac{(2b+2)k_{\text{s}}\Delta t}{\theta_{\text{s}} L} \right]^{-\frac{1}{2b+2}}, \tag{3}$$

where L represents the depth of the rootzone, θ_{t} the soil moisture content at timestep t, b the pore size distribution, k_{s} the saturated conductivity, and Δt the timestep. The value for b is calculated through the clay fraction (CF), using a linear fit based on the values in Clapp and Hornberger (1978):

$$b = 13.52 \cdot \text{CF} + 3.53. \tag{4}$$

Finally, the water balance for the rootzone is defined as follows:

$$\theta_{\text{t+1}} = \theta_{\text{t}} + \Delta t(P_{\text{rain}} + M_{\text{snow}} - ET_{\text{actual}} - Q_{\text{leakage}}), \tag{5}$$

where P_{rain} is the rate of rainfall at timestep t, M_{snow} the rate of snowmelt at timestep t, both are inferred the same way as in the dS2 model (Buitink et al., 2019).

Soil data was obtained from the European Soil Hydraulic Database (EU-SoilHydroGrids ver1.0, Tóth et al., 2017). As this dataset did not contain critical soil moisture contents, it was determined as the mean between wilting point and field capacity. The hygroscopic moisture content was calculted from the moisture retention curve based on Mualem-van Genuchten parameters at -10 MPa (Laio et al., 2001; Tóth et al., 2017). The clay content of the European Soil Hydraulic Database was used to calculate the pore size distribution (b) through a linear fit of the values found in Clapp and Hornberger (1978). For the depth of the rootzone, we chose a depth of 75 cm, but also included simulations ranging from 25 to 125 cm with increments of 25 cm, to account for the uncertainy of this parameter. The potential evaporation input data was calculated using the Penman-Monteith equation (Monteith, 1965), based on ERA5 input data.

Text S1.2, dS2

A conceptual rainfall-runoff model is used to simulate the discharge in the Rhine basin. The dS2 model is based on the simple dynamical systems approach, as proposed by Kirchner (2009). The simple dynamical systems approach is based on the assumption that discharge is a function of storage, such that changes in storage can be related to changes in discharge via a discharge sensitivity function:

$$Q = f(S), \tag{6}$$

$$\frac{\text{d}Q}{\text{d}t} = \frac{\text{d}Q}{\text{d}S}\frac{\text{d}S}{\text{d}t} = \frac{\text{d}Q}{\text{d}S}(P - ET - Q), \tag{7}$$

where Q represents the discharge, S the storage, P and ET the precipitation and actual evaporation, respectively, and $\frac{\text{d}Q}{\text{d}S}$ represent the discharge sensitivity to changes in storage, referred to as $g(Q)$. This concept has been successfully applied and validated in several catchments across Europe (Kirchner, 2009; Teuling et al., 2010; Krier et al., 2012; Brauer et al., 2013; Melsen et al., 2014; Adamovic et al., 2015). Buitink et al. (2019) further developed the concept so it can be applied

in a distributed way, to allow the simulation of larger catchments, while respecting the original scale of development. A new equation to describe the discharge sensitivity is proposed by Buitink et al. (2019), which contains three parameters:

$$g(Q) = e^{\alpha+\beta\ln(Q)+\gamma/Q}. \tag{8}$$

Additionally, the model has been extended with a snow module based on Teuling et al. (2010), and a routing module based on the width function (Kirkby, 1976).

Text S2, Calibration

To calibrate dS2, we optimized the three discharge sensitivity parameters (see Eq. 8), the degree day factor, and an evaporation correction factor. The discharge sensitivity parameters describe how the change in discharge responds to a change in storage, the degree day factor the rate of melting, and the evaporation correction factor is included to correct any bias errors in the forcing data. According to Boussinesq's theory of sloping aquifers (Rupp and Selker, 2006) and the results found in Karlsen et al. (2019), systems with higher slopes are expected to show higher discharge sensitivity values. Therefore, the discharge-sensitivity parameters were defined as a linear function of the slope of each pixel, based on the hypothesis that regions with steeper slopes show a more responsive storage-discharge relation than regions with gentle slopes. This resulted in two fitting parameters (slope and intersect) for each of the three discharge sensitivity parameters. Latin Hypercube sampling was used to gain parameter values evenly sampled across the possible parameter space. The period 2004–2008 was used for calibration. To ensure realistic model performance across the entire basin, the Kling-Gupta efficiency (KGE, Kling and Gupta, 2009) score was calculated at 13 discharge measurement stations within the Rhine basin (see Fig. S1 and Table S1). KGE values across all stations are averaged, and the parameters of each linear fit are used in the following simulations. The degree day factor is assumed constant over the entire basin, and ensures realistic snow melting dynamics. The resulting functions between slope and discharge sensitivity parameters are found, together with the values for the evaporation correction factor (ϵ) and the degree day factor (ddf):

$$\alpha = 0.01381\phi - 3.4240, \tag{9}$$

$$\beta = 0.06790\phi + 0.4036, \tag{10}$$

$$\gamma = 0.03516\phi - 0.1926, \tag{11}$$

$$\epsilon = 1.142\ [-], \tag{12}$$

$$\mathrm{dff} = 3.088\ [\mathrm{mm^{\circ}C^{-1}day^{-1}}], \tag{13}$$

where ϕ represents the slope in degrees.

In Tab. S1, we show the Kling-Gupta efficiencies (KGE) for all basins used in the calibration. The location of these basins within the Rhine is presented in Fig. S1. We also included the KGE for both the 1980s and 2010s period. Due to some limitations in data availability, not all discharge observations covered the entire period. We sliced the timeseries to include most of the available data, yet for some stations it remained impossible to calculate the KGE.

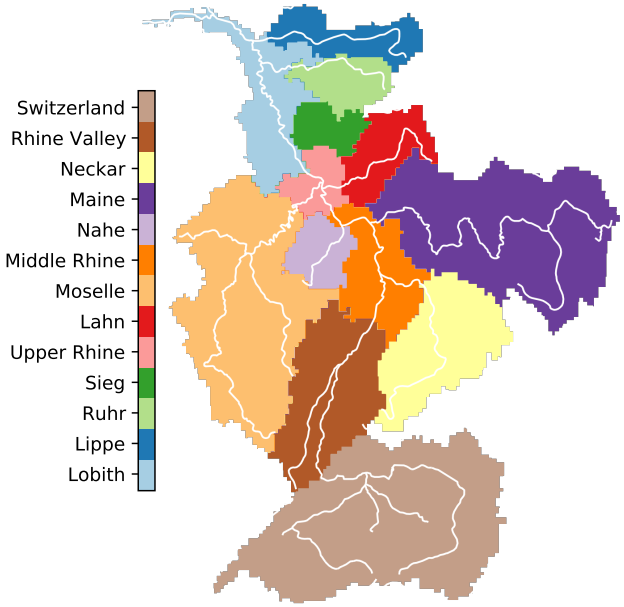

Figure S1. Names and areas corresponding to the (sub-)basins of the Rhine used in this study. The white line indicates the location of the main river network.

Table S1. Model performance statistics over all subbasins in the Rhine basins. Not all basins had sufficient data to cover the simulation periods, the percentage shows fraction of the period covered by the observations.

Basin	Area (km^2)	KGE calib	KGE 1980s	KGE 2010s
Lobith	168448	0.90 (100%)	0.84 (18%)	0.83 (73%)
Lippe	5520	0.44 (100%)	0.32 (9%)	0.45 (74%)
Ruhr	4320	0.80 (100%)	0.63 (2%)	0.87 (76%)
Sieg	3008	0.73 (100%)	0.80 (9%)	0.86 (74%)
Upper Rhine	145984	0.87 (100%)	-	0.88 (73%)
Lahn	5648	0.59 (99%)	0.49 (9%)	0.73 (72%)
Moselle	28272	0.62 (100%)	0.45 (9%)	0.70 (73%)
Middle Rhine	108672	0.87 (100%)	-	0.81 (73%)
Nahe	4032	0.64 (100%)	-	0.76 (76%)
Maine	28800	0.74 (100%)	0.82 (9%)	0.81 (73%)
Neckar	13456	0.74 (99%)	-	0.78 (73%)
Rhine Valley	53872	0.77 (100%)	-	0.75 (73%)
Switzerland	38832	0.71 (19%)	-	0.68 (69%)

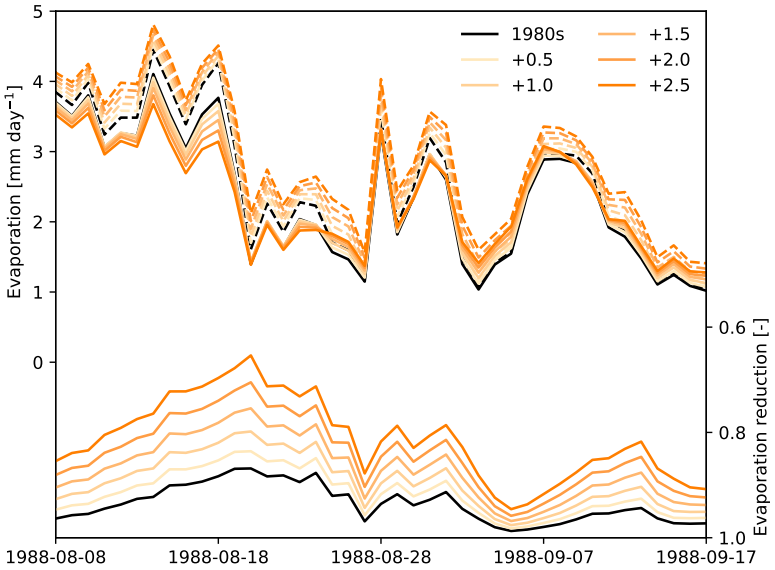

Figure S2. Evaporation differences under increased temperature scenarios. Top half shows potential (dashed) and actual (solid) evaporation, bottom half shows the ratio between actual and potential evaporation. All values are averaged over the entire basin.

Text S3, Temperature induced changes on evaporation and snow

As shown in the manuscript, higher temperatures substantially affect the resulting discharge, where the differences induced by changes in evaporation and snow processes are not constant over the year. To further understand how these processes influence the discharge, the changes in evaporation and snow storage are plotted in Fig. S2 and Fig. S3, respectively.

In Fig. S2, it is visible that potential evaporation will increase with higher temperatures. Despite this, the resulting actual evaporation is not bound to be higher than the 1980s, due to limitations in available soil moisture. This is clearly visible around August 17. Additionally, higher temperatures sometimes hardly change the resulting actual ET, as is the case around August 20. Finally, when sufficient moisture is available for evaporation, higher temperatures will lead to higher actual evaporation rates, as is visible around September 2. The evaporation reduction parameter, indicating the amount of water stress, shows consistently increased reduction with higher temperatures, resulting from the reduced water availability. For most pixels, this relation is non-linear, as it changes from unstressed conditions to water-stressed conditions with higher temperatures.

Unsurprisingly, snow cover and storage shows to be sensitive under higher temperatures. Both the amount of water stored as snow is reduced, as is the fraction of the basin covered with snow. With higher temperatures, a smaller region of the basin is covered with snow. Additionally, the regions that are covered with snow, have less water stored as snow. As a result, the snow storage is also depleted earlier in the year. This is visible in both halves of the figure, where both the snow storage and fractional snow cover reach values close to zero more than one month earlier (mid May 1988 versus late June 1988).

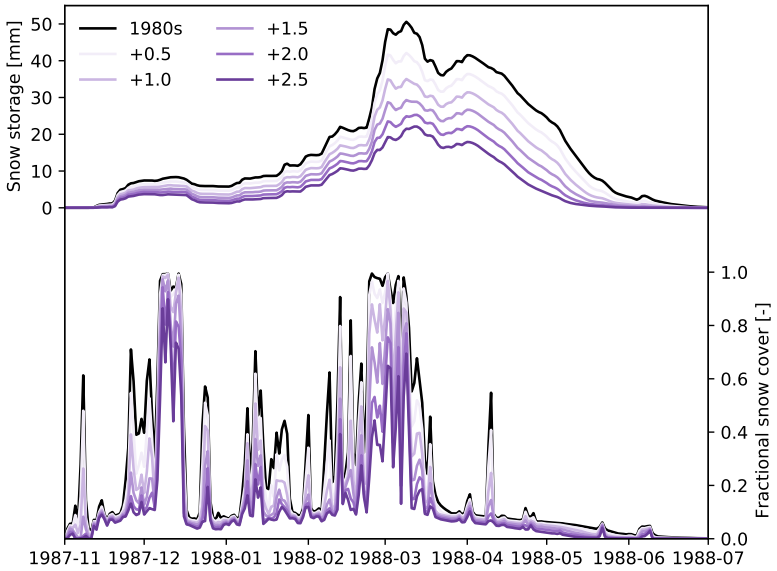

Figure S3. Changes in snow storage and cover under increased temperature scenarios. Top half snow the average amount of water stored as snow in snow-covered pixels, and the bottom half shows the fraction of the basin covered with snow.

References

Adamovic, M., Braud, I., Branger, F., and Kirchner, J. W.: Assessing the Simple Dynamical Systems Approach in a Mediterranean Context: Application to the Ardèche Catchment (France), Hydrology and Earth System Sciences, 19, 2427–2449, https://doi.org/10.5194/hess-19-2427-2015, 2015.

Brauer, C. C., Teuling, A. J., Torfs, P. J. J. F., and Uijlenhoet, R.: Investigating Storage-Discharge Relations in a Lowland Catchment Using Hydrograph Fitting, Recession Analysis, and Soil Moisture Data, Water Resour. Res., 49, 4257–4264, https://doi.org/10.1002/wrcr.20320, 2013.

Buitink, J., Melsen, L. A., Kirchner, J. W., and Teuling, A. J.: A Distributed Simple Dynamical Systems Approach (dS2 v1.0) for Computationally Efficient Hydrological Modelling, Geoscientific Model Development Discussions, pp. 1–25, https://doi.org/10.5194/gmd-2019-150, 2019.

Clapp, R. B. and Hornberger, G. M.: Empirical Equations for Some Soil Hydraulic Properties, Water Resources Research, 14, 601–604, https://doi.org/10.1029/WR014i004p00601, 1978.

Karlsen, R. H., Bishop, K., Grabs, T., Ottosson-Löfvenius, M., Laudon, H., and Seibert, J.: The Role of Landscape Properties, Storage and Evapotranspiration on Variability in Streamflow Recessions in a Boreal Catchment, Journal of Hydrology, 570, 315–328, https://doi.org/10.1016/j.jhydrol.2018.12.065, 2019.

Kirchner, J. W.: Catchments as Simple Dynamical Systems: Catchment Characterization, Rainfall-Runoff Modeling, and Doing Hydrology Backward, Water Resources Research, 45, https://doi.org/10.1029/2008WR006912, 2009.

Kirkby, M. J.: Tests of the Random Network Model, and Its Application to Basin Hydrology, Earth Surface Processes, 1, 197–212, https://doi.org/10.1002/esp.3290010302, 1976.

Kling, H. and Gupta, H.: On the Development of Regionalization Relationships for Lumped Watershed Models: The Impact of Ignoring Sub-Basin Scale Variability, Journal of Hydrology, 373, 337–351, https://doi.org/10.1016/j.jhydrol.2009.04.031, 2009.

Krier, R., Matgen, P., Goergen, K., Pfister, L., Hoffmann, L., Kirchner, J. W., Uhlenbrook, S., and Savenije, H. H. G.: Inferring Catchment Precipitation by Doing Hydrology Backward: A Test in 24 Small and Mesoscale Catchments in Luxembourg, Water Resour. Res., 48, W10 525, https://doi.org/10.1029/2011WR010657, 2012.

Laio, F., Porporato, A., Ridolfi, L., and Rodriguez-Iturbe, I.: Plants in Water-Controlled Ecosystems: Active Role in Hydrologic Processes and Response to Water Stress: II. Probabilistic Soil Moisture Dynamics, Advances in Water Resources, 24, 707–723, https://doi.org/10.1016/S0309-1708(01)00005-7, 2001.

Melsen, L. A., Teuling, A. J., van Berkum, S. W., Torfs, P. J. J. F., and Uijlenhoet, R.: Catchments as Simple Dynamical Systems: A Case Study on Methods and Data Requirements for Parameter Identification, Water Resour. Res., 50, 5577–5596, https://doi.org/10.1002/2013WR014720, 2014.

Monteith, J.: Evaporation and Environment, Symposia of the Society for Experimental Biology, 19, 205–234, 1965.

Rupp, D. E. and Selker, J. S.: On the Use of the Boussinesq Equation for Interpreting Recession Hydrographs from Sloping Aquifers, Water Resources Research, 42, https://doi.org/10.1029/2006WR005080, 2006.

Teuling, A. J., Lehner, I., Kirchner, J. W., and Seneviratne, S. I.: Catchments as Simple Dynamical Systems: Experience from a Swiss Prealpine Catchment, Water Resources Research, 46, https://doi.org/10.1029/2009WR008777, 2010.

Tóth, B., Weynants, M., Pásztor, L., and Hengl, T.: 3D Soil Hydraulic Database of Europe at 250 m Resolution, Hydrological Processes, 31, 2662–2666, https://doi.org/10.1002/hyp.11203, 2017.